科学通报 2016 年 第 61 卷 第 25 期: 2823 ~ 2833
论 文
《中国科学》杂志社
SCIENCE CHINA PRESS

日喀则蛇绿岩白马让岩体的穹窿形结构及构造意义

李源[①*], 李瑞保[②], 董天赐[③], 杨胜标[③], 裴磊[③]

① 中国地质调查局大陆动力学研究中心, 中国地质科学院地质研究所, 北京 100037;
② 长安大学地球科学与资源学院, 西安 710054;
③ 中国地质大学(北京)地球科学与资源学院, 北京 100083
* 联系人, E-mail: liyuancags@126.com

2016-02-17 收稿, 2016-05-16 修回, 2016-05-17 接受, 2016-08-12 网络版发表
中国地质调查局项目(12320115027701, 121201102000150069)资助

摘要 镁铁质岩石出露有限, 超镁铁岩出露厚度大是西藏雅鲁藏布江日喀则蛇绿岩的典型特征. 20世纪80年代中国科学家及中法合作研究以来, 积累了大量岩石学、地球化学和同位素年代学资料, 阐明了该蛇绿岩的基本地质特征, 但是其形成背景一直是争论的焦点. 通过对日喀则蛇绿岩西段白马让岩体地质填图和构造地质学的研究, 从岩体中厘定出2条糜棱岩化蛇纹岩带, 发现岩体具有穹窿形的几何学结构. 研究发现岩体的岩石组合及构造变形特征类似于大洋核杂岩构造: 岩体核部发育高温流动构造的方辉橄榄岩相当于大洋核杂岩核部的大洋岩石圈地幔; 方辉橄榄岩两侧的糜棱岩化蛇纹石带相当于拆离断层带, 拆离断层内发育有强烈变形的辉绿岩、细粒辉长岩和碳酸岩; 拆离断层之上的辉绿岩和玄武岩则相当于拆离断层的上盘. 该成果对于重新理解雅鲁藏布江蛇绿岩成因、多样性, 在造山带厘定和开展大洋核杂岩研究, 以及在造山带中研究岩浆作用与大洋岩石圈伸展构造的相互作用具有重要的理论意义.

关键词 日喀则蛇绿岩, 蛇绿岩构造, 大洋核杂岩, 伸展构造, 拆离断层

西藏日喀则蛇绿岩位于印度板块和欧亚板块汇聚-碰撞过程中形成的雅鲁藏布江缝合带的中段(图1(a)), 是缝合带中保存最完整层序的蛇绿岩[1~4](图1(b)). 作为雅鲁藏布江缝合带中研究程度最高的蛇绿岩, 20世纪80年代中国科学家及中法合作研究[1~4], 阐明了该蛇绿岩的基本地质特征, 但是关于蛇绿岩形成的构造背景这一关键问题备受争议. 包括慢速-超慢速扩张脊[1~5]、接近洋脊与转换断层带交汇处[6]、大陆边缘弧后小洋盆[7,8]、弧前俯冲带环境[9~14]以及由不同构造环境的蛇绿岩块体拼贴组成[15,16]等多种观点, 可以归结为洋中脊(MOR)型和俯冲带(SSZ)型两种类型观点.

持MOR型蛇绿岩观点的研究者提出了大洋慢速-超慢速扩张的构造模型[1~5], 用以解释日喀则蛇绿岩薄壳厚幔的地质现象. 而持SSZ型蛇绿岩观点研究者的主要依据是蛇绿岩的地幔橄榄岩和基性岩石带有与俯冲相关地球化学印记[10,11]. 最近, 在日喀则得几和白朗地区蛇绿岩中发现了少量的玻安质岩石[9,12,13,15], 被认为是类似于IBM初始俯冲带的产物. 然而, 在IBM岛弧带中, 除了玻安质岩外, 还广泛出露岛弧高镁钙碱质火山岩、岛弧拉斑玄武岩和弧前玄武岩[17~19], 而在日喀则蛇绿岩中这类岛弧岩石只有少量出露, 对这些岛弧岩石的野外产出、空间分布、与蛇绿岩镁铁-超镁铁岩的相互关系还不清楚[20].

日喀则蛇绿岩的就位机制被广泛接受的是类似于阿曼蛇绿岩的仰冲就位模式, 即随着65~55 Ma

引用格式: 李源, 李瑞保, 董天赐, 等. 日喀则蛇绿岩白马让岩体的穹窿形结构及构造意义. 科学通报, 2016, 61: 2823–2833
Li Y, Li R B, Dong T C, et al. Structure of the Baimarang massif in the Xigaze ophiolite, Yarlung Zangbo Suture Zone, southern Tibet, China (in Chinese). Chin Sci Bull, 2016, 61: 2823–2833, doi: 10.1360/N972016-00203

© 2016《中国科学》杂志社

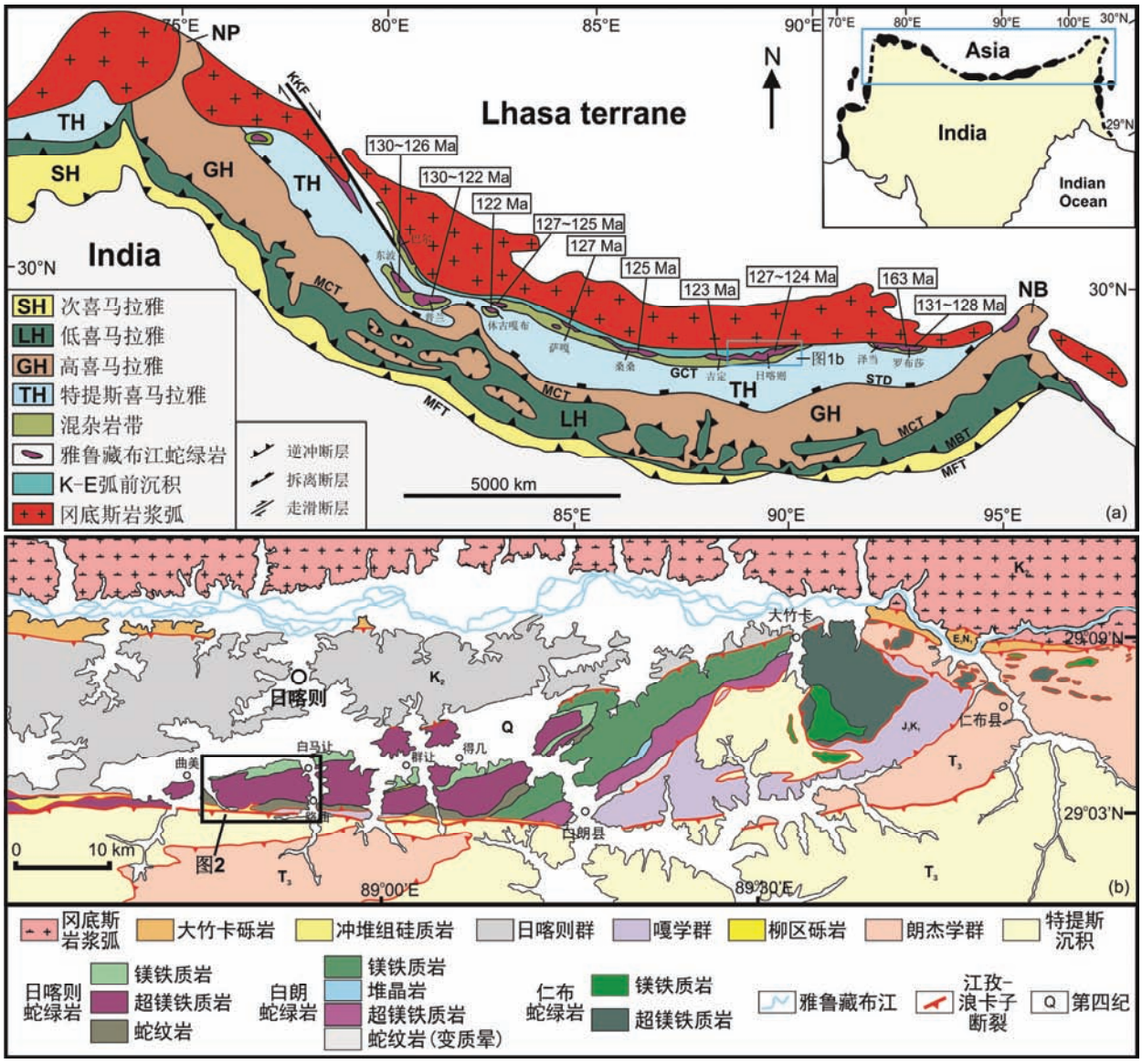


图 1 雅鲁藏布江缝合带与日喀则蛇绿岩地质图. (a) 雅鲁藏布江缝合带地质图(据Xu等人[24]修改简化); NP, 南迦帕尔特构造结; NB, 南迦巴瓦构造结; KKF, 喀喇昆仑断裂; GCT, 大反冲断裂; STD, 藏南拆离断裂; MCT, 主中央冲断裂; MBT, 主边界冲断裂; MFT, 主前冲断裂; (b) 日喀则蛇绿岩地质图(据 1:25 万日喀则地质图和胡敬仁等人[16]修改)

Figure 1 Distribution of the Yarlung Zangbo ophiolites, Tibet and their U-Pb age of zircon from mafic rocks and map of Xigaze ophiolite. (a) Schematic tectonic map of southern Tibet (after Xu et al.[24]); NP, Nanga Parbat syntaxis; NB, Namche Barwa syntaxis; KKF, Karakorum fault; GCT, Great Counter thrust; STD, South Tibet detachment; MCT, Main Central thrust; MBT, Main Boundary thrust; MFT, Main Front thrust; (b) geological map of the Xigaze ophiolite

的印度-亚洲碰撞, 残余的新特提斯洋洋壳向南仰冲到印度板块前缘的被动陆缘上, 形成北倾南冲的构造岩片[21~24]. 日喀则蛇绿岩的就位时间主要通过蛇绿岩底部变质底板来约束. Malpas等人[25]获得白朗地区蛇绿岩变质底板角闪岩的角闪石^{40}Ar-^{39}Ar年龄(88 Ma), 认为代表了蛇绿岩构造侵位的年龄. Guilmette等人[26,27]获得昂仁-白朗-桑桑-萨嘎地区蛇绿岩变质底板中石榴石斜长角闪岩的角闪石^{40}Ar-^{39}Ar年龄(132~123 Ma), 指出变质底板是先成的洋壳受到热幔的烘烤而形成, 认为蛇绿岩在形成不久, 就侵位于洋内俯冲形成的弧前位置. 该变质年龄与Dai等人[12]获得的日喀则得几玻安岩的锆石U-Pb年龄(127±3.5 Ma)在相同的范围内. 由于玻安质岩石的生成环境本身就具有高地温梯度的特征, 因此该变质年龄也可

能代表的是俯冲起始的时间. 最近, 刘小汉等人[8]通过对雅鲁藏布江(以下简称雅江)蛇绿岩两侧的构造剖面和地层的对比, 对仰冲就位模式提出了质疑, 认为日喀则白朗和仁布地区的蛇绿岩可能是形成于弧后盆地的原地系统, 而非经历俯冲-碰撞-反逆冲作用的外来的残余洋壳岩片.

上述的这些观测结果表明日喀则蛇绿岩的构造背景具有特殊性, 而岩石组合的野外产出、空间分布和相互关系不清等问题, 已经制约了对蛇绿岩成因的全面解析. 对日喀则蛇绿岩开展精细的地质填图和构造地质学研究, 厘定蛇绿岩不同构造单元之间的相互关系以及形成、就位过程中构造变形形迹, 有助于提升对日喀则蛇绿构造、形成背景及就位机制等关键问题的认识.

1 地质背景

西藏日喀则蛇绿岩位于雅鲁藏布江缝合带中段(图1(a)), 主要由日喀则蛇绿岩体、白朗蛇绿岩体和仁布岩体3个岩体组成(图1(b)). 日喀则蛇绿岩北部与晚白垩世复理石沉积日喀则群相邻, 南侧与上侏罗-下白垩统嘎学群呈断层接触或被古近纪柳区砾岩角度不整合覆盖(图1(b)), 保存了完整的蛇绿岩层序, 具备雅鲁藏布江蛇绿岩的典型特征: (1) 镁铁质岩出露有限, 而超镁铁岩出露厚度大; (2) 大量的辉绿岩脉不但侵入到上部的玄武岩之中, 还侵入于地幔橄榄岩之中[1~4]; (3) 镁铁质岩石的同位素年代学集中在130~122 Ma狭窄的范围内[5,11,24].

2 日喀则蛇绿岩白马让岩体的构造研究

作者在参加中国地质调查局“西藏日喀则岩体及其外围岩体铬铁矿调查”项目期间, 对日喀则蛇绿岩的白马让岩体开展了蛇绿岩构造研究和1∶5万地质填图(图2), 详细划分了岩石类型, 将蛇绿岩体细化为2个填图单元、3层结构(表1). 从蛇绿岩体中厘定出2条糜棱岩化蛇纹岩带, 发现白马让蛇绿岩体具有穹窿形的空间几何学形态.

2.1 沉积地层

硅质岩(K_1Si)在研究区只有极少出露, 呈薄层状连续沉积在气孔-杏仁状玄武岩之上, 最宽处不足10 m, 与日喀则群复理石没有直接接触, 产状60°(NW)∠70°. 从其产出位置和与蛇绿岩的接触关系来看, 应属于群让冲堆组[28].

2.2 镁铁质岩石单元

研究区的镁铁质岩石主要为辉绿岩, 另有少量的玄武岩和辉长岩. 从产状上可分为火山岩和侵入岩两种类型(表1), 没有发现堆晶岩. 火山岩包括枕状玄武岩和气孔-杏仁状玄武岩岩流两种类型, 枕状玄武岩只在岩体最北部有少量出露; 气孔-杏仁状玄武熔岩产状60°(NW)∠75°, 与上部硅质岩产状基本一致, 被日喀则复理石整合覆盖(图3(a)).

研究区侵入岩出露于玄武岩和超镁铁岩之间, 主要在超镁铁岩的北侧出露, 南侧仅有极少出露. 侵

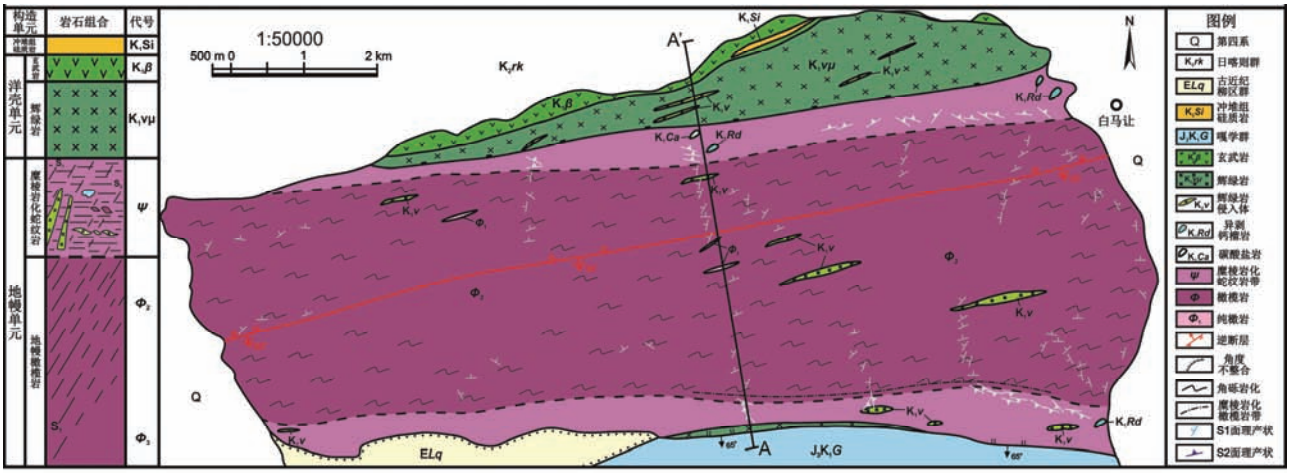


图 2 日喀则蛇绿岩白马让岩体 1∶50000 地质简测图

Figure 2 Schematic map of the Baimarang massif from the Xigaze ophiolite

表 1 日喀则蛇绿岩白马让岩体填图单位划分表

Table 1 The mapping units of Baimarang massif, Xigaze ophiolite

填图单元	岩石类型	填图单位		岩石组合	备注
沉积地层	洋壳沉积	K_1Si		硅质岩组合	紫红色、青灰色硅质板岩
镁铁质岩	镁铁质岩浆岩	火山岩	$K_1\beta^p$	枕状玄武岩	
			$K_1\beta^m$	块状玄武岩	枕状玄武岩和气孔-杏仁状玄武岩较多，块状和角砾状玄武岩较少
			$K_1\beta^v$	气孔-杏仁状玄武岩	
			$K_1\beta^b$	角砾状玄武岩	
		侵入岩	$K_1\beta\mu$	辉绿岩	层状、岩墙和岩脉
			$K_1\nu$	细粒辉长岩	岩脉
超镁铁岩	糜棱岩化蛇纹岩带	Ψ		蛇纹岩、辉绿岩脉、异剥钙榴岩、碳酸岩	糜棱岩化、碎裂岩化
	新鲜橄榄岩	Φ_1		纯橄岩	岩脉或透镜体
		Φ_2		方辉橄榄岩	高温流变
		Φ_3		二辉橄榄岩	常含辉石岩和纯橄岩脉

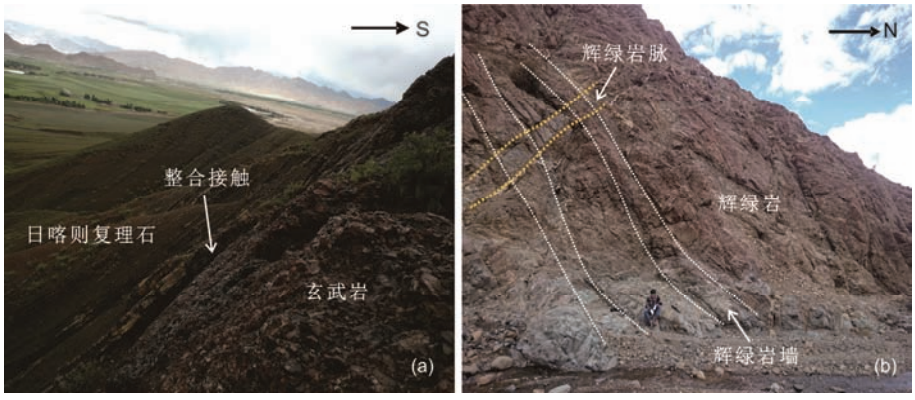


图 3 日喀则蛇绿岩白马让岩体镁铁质岩野外照片. (a) 日喀则复理石整合覆盖在玄武岩之上; (b) 白马让岩体中的辉绿岩、辉绿岩墙与辉绿岩脉

Figure 3 Field photographs of the mafic rocks from the Baimarang massif, Xigaze ophiolite. (a) Basalt conformably covered by the Xigaze group; (b) doleritic dike within dolerite

入岩主要为辉绿岩，可见少量的细粒角闪辉长岩脉侵入其中. 辉绿岩与上覆玄武岩呈过渡接触，辉绿岩中有两种产状的辉绿岩脉体(图3(b)): 一种呈多条岩墙平行产出，可见单侧冷凝边，产状60°(NW)∠65°，近平行于玄武熔岩和硅质岩；第二种与第一种近垂直，产状75°(S)∠55°.

2.3 超镁铁岩单元

依据超镁铁岩的产状特征，分为核部的新鲜橄榄岩及其两侧的糜棱岩化蛇纹岩两部分.

(ⅰ) 新鲜橄榄岩. 研究区新鲜橄榄岩南北向宽5~6 km，依据橄榄岩的矿物组合可细分为纯橄岩、方辉橄榄岩、二辉橄榄岩3个端元(表1). 核部的橄榄岩最新鲜，岩石流动构造较弱，主要为含透辉石的方辉橄榄岩和少量二辉橄榄岩(图4(a))，二者之间的界限难以区分. 由核部向外，橄榄岩新鲜程度降低，透辉石含量减少，逐渐过渡为亏损的方辉橄榄岩(图5(a)). 方辉橄榄岩具有明显的高温流动构造(图4(b))，流面(S1)优势产状北西倾，倾角大部分介于60°~80°间(图5(b)-③). 岩石流线主要由铬尖晶石的定向排列显示，大致为北西或西倾，倾角变化较大介于30°~50°之间，指示了一个向上和向北的相对运动[4]. 新鲜橄榄岩中局部可见切穿方辉橄榄岩S1面理的辉石岩(图4(c))和平行于S1面理的纯橄岩(图4(d))，这种构造与阿尔卑斯等地区的橄榄岩中的构造相似，暗示橄榄岩受到过流体或熔体的交代作用[29~32].



图 4 日喀则蛇绿岩白马让岩体橄榄岩野外照片. (a) 二辉橄榄岩; (b) 方辉橄榄岩的高温流动构造构成S_1面理; (c) 辉石岩脉切穿方辉橄榄岩S_1面理; (d) 平行于方辉橄榄岩S_1面理的纯橄岩脉

Figure 4 Field photographs of the ultra-mafic rocks from the Baimarang massif, Xigaze ophiolite. (a) Lherzolite; (b) harzburgite display a clear foliation S_1; (c) pyroxenite cut the primary S_1 foliation; (d) dunite parallel to the primary S_1 foliation

(ⅱ) 糜棱岩化蛇纹岩带. 糜棱岩化蛇纹岩单元分布在新鲜橄榄岩的南北两侧, 呈过渡接触. 本单元的显著特征是发育大量的辉绿岩脉, 局部可见强烈变形的碳酸岩(图6(a)). 本单元在南北方向上呈现出变形分带的现象. 靠近镁铁质岩单元, 蛇纹岩碎裂岩化较强. 在核部, 则全部为糜棱岩化蛇纹岩, 辉绿岩脉(图6(b), (d))和残留的糜棱岩化橄榄岩碎斑(图6(e))也强烈变形, 呈石香肠构造.

北侧的糜棱岩化蛇纹岩带与上覆的辉绿岩接触关系似乎是过渡的, 二者间的接触面产状不稳定, 平均60°(NW)∠50°. 糜棱岩化蛇纹岩的面理向北或北西倾, 倾角介于50°~70°间(图5(b)-⑥). 蛇纹岩中辉绿岩布丁(图6(b))AB面的产状与糜棱岩化蛇纹岩面理基本一致, 北或北西倾, 倾角55°~70°(图6(b)-⑤).

南侧的糜棱岩化蛇纹岩带向南与上侏罗-下白垩统嘎学群(J_3k_1G)放射虫硅质岩呈断层接触(图6(c)). 该蛇纹岩带曾被称为“构造角砾岩带”或“蛇绿质混杂岩带”, 被认为是蛇绿岩就位过程中形成的“搬运面”或特提斯洋俯冲时在雅江南侧形成的增生杂岩体[2,28]. 该带与北侧的糜棱岩化蛇纹岩带具有相同的岩石组合, 但变形程度更强. 糜棱岩化蛇纹岩面理倾向南东, 倾角60°~70°(图5(b)-①). 辉绿岩旋转布丁AB面的倾向南或南东, 倾角50°~70°(图5(b)-②). 辉绿岩σ型旋转布丁(图6(d))和糜棱岩化橄榄岩碎斑系指示糜棱岩带具有正断层的性质, 剪切指向自北向南. 在该带的顶部, 有一条宽2~3 m的橄榄岩糜棱岩带(图6(f)), 与核部的新鲜橄榄岩均呈过渡接触, 面理140°(SW)∠65°, 拉伸线理160°(SE)∠25°, 指示一个自北向南的运动, 与底部糜棱岩带运动指向基本一致.

(ⅲ) 橄榄岩糜棱岩的显微构造. 橄榄岩糜棱岩原岩为方辉橄榄岩, 具糜棱结构、残斑结构. 主要矿物为橄榄石(70%~80%)、顽火辉石(15%~25%)和少量的透辉石(<5%), 副矿物为铬尖晶石. 残斑晶为拉长的顽火辉石和少量的单斜辉石集合体(图7(a), (b)). 基质矿物含量>50%, 主要为动态重结晶的细粒橄榄

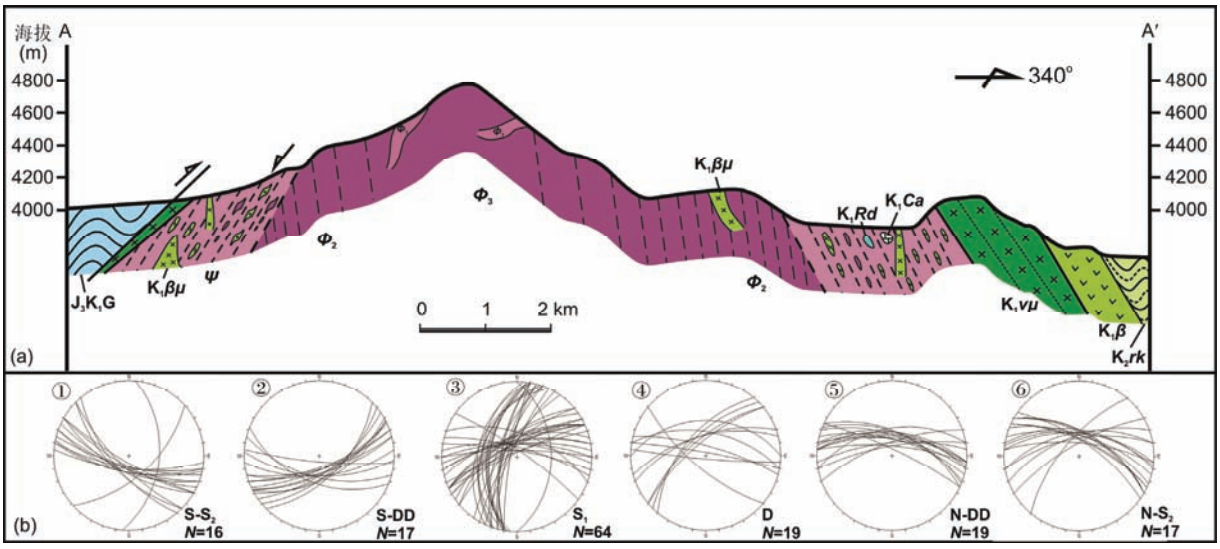


图 5 日喀则蛇绿岩白马让岩体构造剖面图和产状要素. (a) 构造剖面图. J_3K_1G, 上侏罗-下白垩系嘎学群; $K_1\beta\mu$, 辉绿岩脉; ψ, 糜棱岩化蛇纹岩; Φ_1, 纯橄岩; Φ_2, 方辉橄榄岩; Φ_3, 二辉橄榄岩; K_1Ca, 碳酸岩; K_1Rd, 异剥钙榴岩; $K_1v\mu$, 辉绿岩; $K_1\beta$, 玄武岩; K_2rk, 上白垩系日喀则复理石; MP, 橄榄岩糜棱岩. (b) 产状要素图: ①-南侧糜棱岩化蛇纹岩面理S_2产状(S-S_2); ②-南侧糜棱岩化蛇纹岩带中辉绿岩脉布丁AB面产状(S-DD); ③-橄榄岩流面S_1产状; ④-新鲜橄榄岩中辉绿岩脉产状(D); ⑤-北侧糜棱岩化蛇纹岩带中辉绿岩脉布丁AB面产状(N-DD); ⑥-北侧糜棱岩化蛇纹岩面理S_2产状(N-S_2). 产状要素测量位置见图 2

Figure 5 Cross section and structural elements for the Baimarang massif, Xigaze. (a) Cross section. J_3K_1G, upper Jurassic-Lower Cretaceous Gaxue group; $K_1\beta\mu$, early Cretaceous dolerite; ψ, mylonitic serpentinite; Φ_1, dunite; Φ_2, harzburgite; Φ_3, lherzolite; K_1Ca, Early Cretaceous carbonatite; K_1Rd, Rodingite; $K_1\beta$, Early Cretaceous basalts; K_2rk, upper Cretaceous Xigaze group; MP, peridotite mylonite. (b) Structural elements for the Baimarang massif, Xigaze. ① Southern side mylonitic serpentinite of the Bamarang massif display a clear foliation S_2 (16 measurements); ② dolerite boudin in the Southern side mylonitic serpentinite of the Bamarang massif (17 measurements); ③ S_1 foliation (64 measurements); ④ undeformed dolerite in the fresh peridotite (19 measurements); ⑤ dolerite boudin in the Northern side mylonitic serpentinite of the Bamarang massif (19 measurements); ⑥ northern side mylonitic serpentinite of the Bamarang massif display a clear foliation S_2 (17 measurements)

石, 内部波状消光不发育. 透辉石和尖晶石呈细小颗粒分布在顽火辉石残斑周围, 或基质橄榄石中. 岩石的显微构造受到定向拉长的顽火辉石残斑、平行相间的条带状或细粒橄榄石的控制. 顽火辉石残斑晶显示明显的膨凸重结晶现象, 内部发育单斜辉石的出溶页片和尖棱状的扭折变形(图7(c)), 少量的出溶页片发生弯曲变形, 指示右行的剪切作用(图7(d)).

3 讨论与结论

通过细致的填图和构造地质学研究, 可以发现日喀则蛇绿岩白马让岩体是一个镁铁质岩石单元构造简单、超镁铁岩单元内部构造复杂、具有不对称结构的“蛇绿岩穹窿”, 暗示其形成在构造伸展的背景下. 穹窿的核部为高温流变的橄榄岩, 幔部为糜棱岩化的橄榄岩和蛇纹岩, 边部为脆性破裂的镁铁质岩.

大洋岩石圈的形成是构造伸展和岩浆作用相互作用的结果. 中-快速扩张脊背景下, 岩浆供给充足, 沿扩张中心走向会形成一套连续的岩浆岩建造, 如Oman的Semail蛇绿岩[33,34]. 在慢速扩张洋脊的背景下, 扩张作用主要受构造控制, 蛇绿岩具有复杂的地幔结构, 但是由于岩浆的供给有限, 很难形成复杂的洋壳结构[35].

Dick等人[36]首次在慢速扩张的大西洋中脊Kane转换断层附近发现了大型拆离断层. 拆离断层由强烈蛇纹石化的橄榄岩、超镁铁质糜棱岩、糜棱岩化辉长岩和碳酸岩等组成[37], 蛇纹石化前锋可能是拆离断层根部的流变学边界[38]. 拆离断层可分为两个端元类型[39]: (1) 高温型, 具有广泛的糜棱岩化(800~900℃), 如西南印度洋的Atlantis Bank; (2) 低温型, 以滑石-透闪石-绿泥石-蛇纹石片岩为特征, 下盘无糜棱岩化作用(如大西洋30°N). 拆离断层的持续活动导致大洋岩石圈深部的地幔橄榄岩以不对称的构造样式暴露于洋底[40~46]. 拆离断层的活动往往伴随大洋核杂岩(Oceanic Core Complex)的形成.

对比慢速扩张脊大洋核杂岩的构造, 可以发现日喀则蛇绿岩白马让“蛇绿岩穹窿”与形成在慢速-超

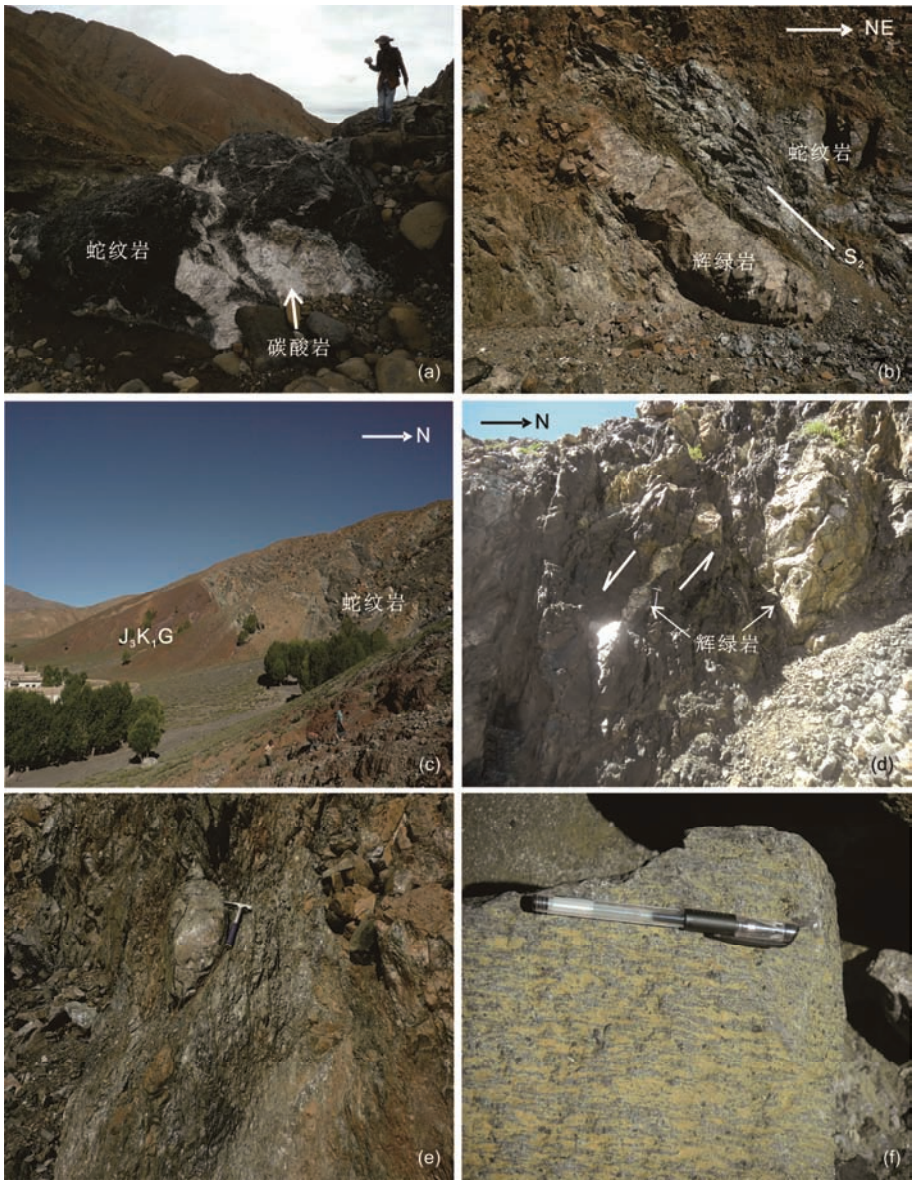


图 6 日喀则蛇绿岩白马让岩体糜棱岩化蛇纹岩野外照片. (a) 糜棱岩化蛇纹岩中的碳酸岩; (b) 新鲜橄榄岩北侧的糜棱岩化蛇纹岩和同构造变形辉绿岩; (c) 新鲜橄榄岩南侧的糜棱岩化蛇纹岩带与上侏罗-下白垩统嘎学群(J_3K_1G)呈断层接触; (d) 南侧糜棱岩化蛇纹岩中的同构造辉绿岩σ型旋转布丁指示向南运动; (e) 糜棱岩化蛇纹岩中的辉橄岩碎斑; (f) 南侧糜棱岩化蛇纹岩带顶部的橄榄岩糜棱岩

Figure 6 Field photographs of mylonitic serpentinite from the Baimarang massif, Xigaze ophiolite. (a) Carbonatite with in mylonitic serpentinite; (b) syntectonic deformation within the Northern side mylonitic serpentinite; (c) structural contact between the southern side mylonitic serpentinite and Upper Jurassic-Lower Cretaceous Gaxue group; (d) σ-type dolerite boudins in the Southern side mylonitic serpentinite indicate a southward movement of the overlying unit relative to the underlying fresh peridotite; (e) peridotite lense within the southern side mylonitic serpentinite; (f) peridotite mylonite overlying the southern side mylonitic serpentinite

慢速洋脊背景下的大洋核杂岩, 具有相似的岩石组合和内部构造特征(表2). 日喀则白马让岩体的新鲜橄榄岩相当于大洋核杂岩核部的大洋岩石圈地幔. 新鲜橄榄岩两侧的糜棱岩化橄榄岩和蛇纹岩带相当于拆离断层带. 拆离断层内发育有强烈变形的辉绿岩、细粒辉长岩和碳酸岩. 拆离断层具有广泛的糜棱岩化和蛇纹岩化, 显微构造显示橄榄岩的剪切变形作用类型与西南印度洋大洋核杂岩中发育的拆离断层相似, 属于高温型拆离断层.

Liu等人[47]和Maffione等人[14]在对普兰和日喀则蛇绿岩研究时, 利用地球化学和古地磁证据, 提出过雅鲁藏布江蛇绿岩的大洋核杂岩和拆离断层成因模

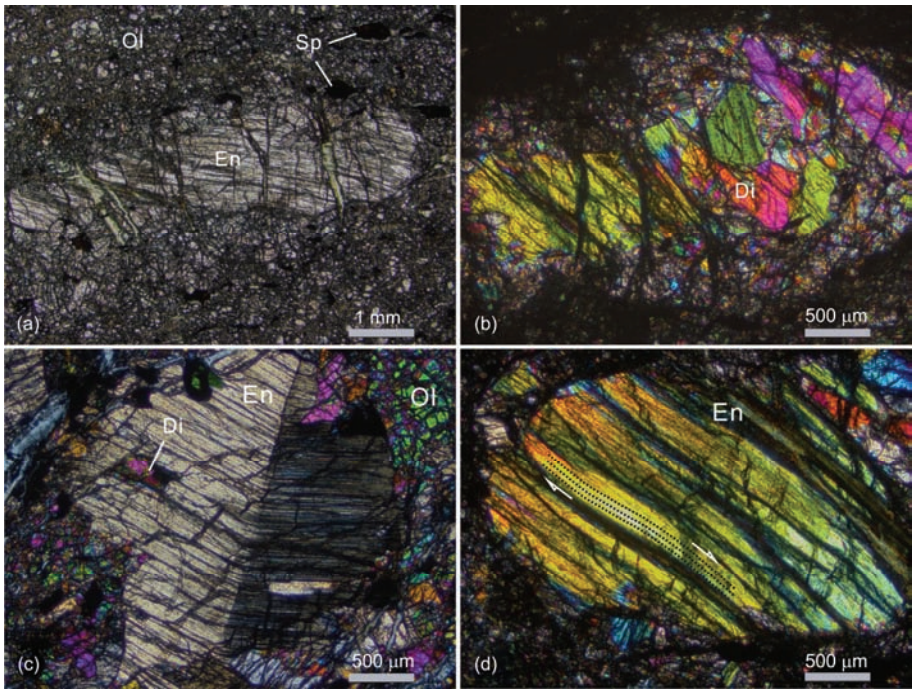


图 7 橄榄岩糜棱岩的显微照片. (a) 橄榄岩糜棱岩具残斑结构, 残斑为拉长的顽火辉石, 定向排列的尖晶石分布在顽火辉石周围, 或橄榄石基质中; (b) 橄榄岩糜棱岩的透辉石集合体残斑; (c) 顽火辉石残斑中普遍发育单斜辉石出溶页片和尖棱状扭折变形; (d) 顽火辉石中单斜辉石出溶页片的弯曲方向指示右行的剪切作用

Figure 7 Micro structure photomicrographs of the peridotite mylonite. (a) Porphyroclastic texture in the peridotite mylonite; (b) aggregate of the diopside in the peridotite mylonite; (c) deformed enstatite porphyroclast; (d) the enstatite porphyroclast deformed by gliding due to a dextral simple shear

表 2 日喀则蛇绿岩白马让岩体与大洋核杂岩特征对比

Table 2 Comparative study between the Baimarang massif, Xigaze ophiolite, and the oceanic core complex from the slow-spreading ridge

	白马让岩体	大洋核杂岩[37~47]
形态和构造特征	穹隆状不对称构造、低-中高角度正断层	穹窿状不对称构造、窗棱构造、低角度正断层
岩石组合	下盘: 不同程度蛇纹石化的橄榄岩、辉绿岩脉; 上盘: 辉绿岩、玄武岩	下盘: 蛇纹石化橄榄岩、纯橄岩、橄长岩、辉长岩等; 上盘: 火山沉积、熔岩流、辉绿岩墙
拆离断层构造岩	糜棱岩化橄榄岩、糜棱岩化蛇纹岩	糜棱岩化蛇纹岩、糜棱岩化辉长岩、角砾岩、微角砾岩
拆离断层类型	高温型: 具有广泛的糜棱岩化	高温型: 具有广泛的糜棱岩化; 低温型: 以滑石-透闪石-绿泥石-蛇纹石片岩为特征, 无糜棱岩化作用

型, 但是还缺少关键的构造地质学证据. 日喀则白马让的“穹窿”形结构和拆离断层的厘定, 对于重新理解雅江蛇绿岩的成因和多样性、在造山带厘定和开展大洋核杂岩研究具有重要的理论意义.

致谢 感谢两位审稿人的建设性意见, 对本文大有裨益. 在成文过程中, 与中国地质科学院地质研究所李化启、董汉文进行过有益的讨论, 在此一并致谢.

参考文献

1 Nicolas A, Girardeau J, Marcoux J, et al. The Xigaze ophiolite (Tibet): A peculiar oceanic lithosphere. Nature, 1981, 294: 414–417

2 Girardeau J, Mercier J C C. Structure of the Xigaze ophiolite, Yarlung Zangbo Suture Zone, southern Tibet, China: Genetic implication. Tectonics, 1985, 4: 267–288

3 Wang X B, Bao P S, Xiao X C, et al. Ophiolite of the Yarlung Zangbo River, Xizang (in Chinese). Beijing: Publishing House of Surveying and Mapping, 1987. 1–118 [王希斌, 鲍佩声, 肖序常, 等. 西藏雅鲁藏布蛇绿岩. 北京: 测绘出版社, 1987. 1–118]

4 Nicolas A. Structure of ophiolites and dynamics of oceanic lithosphere. Petrol Struct Geol, 1989, 4: 91–104

5 Wu F Y, Liu C Z, Zhang L L, et al. Yarlung Zangbo ophiolite: A critical updated view (in Chinese). Acta Petrol Sin, 2014, 30: 293–325 [吴福元, 刘传周, 张亮亮, 等. 雅鲁藏布江蛇绿岩——事实与臆想. 岩石学报, 2014, 30: 293–325]

6 Pearce J A, Deng W. The ophiolites of the Tibetan Geotraverses, Lhasa to Golmud (1985) and Lhasa to Kathmandu (1986). Philos Trans R Soc London Ser A, 1988, 327: 215–238

7 Xiao X C, Wang J. A brief review of tectonic evolution and uplift of the Qinhai-Tibet Plateau (in Chinese). Geol Rev, 1998, 4: 372–381 [肖序常, 王军. 青藏高原构造演化及隆升的简要评述. 地质论评, 1998, 4: 372–381]

8 Liu X H, Li G W, Liu X B, et al. Regional tectono-sedimentary feature of the Yarlung Zangbo Suture zone (in Chinese). Chin J Geol, 2009, 44: 1312–1326 [刘小汉, 李广伟, 刘小兵, 等. 雅鲁藏布缝合带区域性构造-沉积特征. 地质科学, 2009, 44: 1312−1326]

9 Chen G W, Xia B, Zhong Z H, et al. Geochemical characteristics and geological significance of Boninites in the Deji ophiolite, Tibet (in Chinese). Acta Mineral Sin, 2003, 23: 91–96 [陈根文, 夏斌, 钟志洪, 等. 西藏得几蛇绿岩体中玻安岩的地球化学特征及其地质意义. 矿物学报, 2003, 23: 91–96]

10 Wang C S, Li Y L, Liu Z F, et al. Yalung Zangbo ophiolites revisited from geological survey to mineral records (in Chinese). Acta Geol Sin, 2005, 79: 323–330 [王成善, 李亚林, 刘志飞, 等. 雅鲁藏布江蛇绿岩再研究: 从地质调查到矿物记录. 地质学报, 2005, 79: 323–330]

11 Hébert R, Huot F, Guilmette C, et al. The Indus-Yarlung Zangbo ophiolites from Nanga Parbat to Namche Barwa Syntaxes, southern Tibet: First synthesis of petrology, geochemistry, and geochronology with incidences on geodynamic reconstrutions of Neo-Thethys. Gondwana Res, 2012, 2: 377–397

12 Dai J G, Wang C S, Polat A, et al. Rapid forearc spreading between 130–120 Ma: Evidence from geochronology and geochemistry of the Xigaze ophiolite, Southern Tibet. Lithos, 2013, 172-173: 1–16

13 Bao P S, Su L, Wang J, et al. Study on the tectonic setting for the ophiolites in Xigaze. Acta Geol Sin, 2013, 87: 395–427

14 Maffione M, Douwe J J, van Hinsbergen, et al. Forearc hyperextension dismembered the south Tibetan ophiolites. Geology, 2015, 43: 475–478

15 Zhang Q, Zhou G Q. Ophiolites of China (in Chinese). Beijing: Science Press, 2001. 1–182 [张旗, 周国庆. 中国蛇绿岩. 北京: 科学出版社, 2000. 1–182]

16 Hu J R, Sun Z L, Chen G J, et al. New results and major progress in regional geological survey of the Xigaze City Sheet (in Chinese). Geol Bull China, 2004, 23: 463–470 [胡敬仁, 孙中良, 陈国结, 等. 日喀则市幅地质调查新成果及主要进展. 地质通报, 2004, 23: 463–470]

17 Ishizuka O, Kimura J, Li Y B, et al. Early stages in the evolution of Izu-Bonin arc volcanism: New age, chemical, and isotopic constrains. Earth Planet Sci Lett, 2006, 250: 385–401

18 Ishizuka O, Reagan M K, Kanayama K, et al. The timescale of subduction initiation and subsequent evolution of an oceanic island arc. Earth Planet Sci Lett, 2011, 306: 229–240

19 Reagan M K, Ishizuka O, Stern R J, et al. Fore-arc basalts and subduction initiation in the Izu-Bonin-Mariana system. Geochem Geophys Geosys, 2010, 11: 427–428

20 Zhang Q. Some problems on the Xigaze ophiolite (in Chinese). Acta Petrol Sin, 2015, 31: 37–46 [张旗. 日喀则蛇绿岩研究中的几个问题. 岩石学报, 2015, 31: 37–46]

21 Allègre C J, Courtillot V, Tapponnier P, et al. Structure and evolution of the Himalaya-Tibet orogenic belt. Nature, 1984, 307: 17–22

22 Huot F, Hébert R, Varfalvy V, et al. The Beimarang mélange (southern Tibet) brings additional constraints in assessing the origin, metamorphic evolution and obduction processes of the Yarlung Zangbo ophiolite. J Asian Earth Sci, 2002, 21: 307–322

23 Ding L, Kapp P, Wan X. Paleocene-Eocene record of ophiolite obduction and initial India-Asia collision, south central Tibet. Tectonics, 2005, 24: 1–18

24 Xu Z Q, Dilek Y, Yang J S, et al. Crustal structure of the Indus-Tsangpo suture zone and its ophiolite in southern Tibet. Gondwana Res, 2015, 27: 507–524

25 Malpas J, Zhou M F, Robinson P T, et al. Geochemical and geochronological constraints on the origin and emplacement of the Yarlung Zangbo ophiolites, Southern Tibet. In: Dilek Y D, Robinson P T, eds. Ophiolites in Earth History. London: Geological Society of London, 2003. 191–206

26 Guilmette C, Hébert R, Wang C S, et al. Geochemistry and geochronology of highly foliated amphibolites from the ophiolitic mélange, Xigaze area, Yarlung Zangbo Suture Zone. Lithos, 2009, 112: 149–162

27 Guilmette C, Hébert R, Dostal J, et al. Discovery of a dismembered metamorphic sole in the Saga ophiolitic mélange, South Tibet: Assessing an Early Cretaceous disruption of the Neo-Tethyan supra-subduction zone and consequences on basin closing. Gondwana Res, 2012, 22: 398–414

28 Wang C S, Liu Z F, Li X H, et al. Xigaze forearc basin and Yarlung Zangbo Suture Zone, Tibet (in Chinese). Beijing: Geological Publishing House, 1999. 112–200 [王成善, 刘志飞, 李祥辉, 等. 西藏日喀则弧前盆地与雅鲁藏布江缝合带. 北京: 地质出版社, 1999. 112–200]

29 Garrido C J, Bodinier J L. Diversity of mafic rocks in the Ronda peridotite: Evidence for pervasive melt-rock reaction during heating of subcontinental lithosphere by upwelling asthenosphere. J Petrol, 1999, 40: 729–754

30 Bodinier J L, Godard M. Orogenic, ophiolitic, and abyssal peridotites. In: Holland H D, Turekian K K, eds. Treatise on Geochemistry. New York: Elsevier, 2003, 2: 103–170

31 Boudier J L, Garrido C, Chanefo I, et al. Origin of pyroxenite-peridotite veined mantle by refertilization reactions: Evidence from the Ronda Peridotite (Southern Spain). J Petrol, 2008, 49: 999–1025

32 Gysi A P, Jagoutz O, Schmedt M M, et al. Petrogenesis of pyroxenites and melt infiltrations in the ultramafic complex of Beni Bousera, northern Morocco. J Petrol, 2011, 52: 1679–1735

33 Nicolas A, Reuber I, Benn K. A new magma chamber model based on structural studies in the Oman ophiolite. Tectonophysics, 1988, 151: 27–56

34 Boudier F, Nicolas A, Ildefonse B. Magma chambers in the Oman ophiolite: Fed from the top and the bottom. Earth Planet Sci Lett, 1996, 144: 239–250

35 Karson J A. Seafloor spreading on the Mid-Atlantic Ridge: Implications for the structure of ophiolites and oceanic lithosphere produced in slow-spreading environments. In: Malpas J, ed. Ophiolites Oceanic Crustal Analogues, 1990. 547–556

36 Dick H J B, Bryan W, Thompson G. Low-angle faulting and steady-state emplacement of plutonic rocks at ridge-transform intersections. Eos Trans AGU, 1981, 62: 406

37 Macleod C, Escartin J, Banerji D, et al. Direct geological evidence for oceanic detachment faulting: The Mid-Atlantic Ridge, 15°45′N. Geology, 2002, 30: 879–882

38 Li S Z, Lü H Q, Hou F H, et al. Oceanic core complex (in Chinese). Mar Geol Quat Geol, 2006, 26: 47–52 [李三忠, 吕海清, 侯方辉, 等. 海洋核杂岩. 海洋地质与第四纪地质, 2006, 26: 47–52]

39 McCaig A M, Delacour A, Fallick A E, et al. Detachment fault control on hydrothermal circulation systems: Interpreting the subsurface beneath the TAG hydrothermal field using the isotopic and geological evolution of Oceanic Core Complexes in the Atlantic. In: Rona P A, Devey C W, Dyment J, et al., eds. Diversity of Hydrothermal Systems on Slow Spreading Ocean Ridges. Washington DC: AGU, 2010

40 Cann J R, Smith D K, McAllister E, et al. Corrugated slip surfaces formed at North Atlantic ridge-transform intersections on the Mid-Atlantic Ridge. Nature, 1997, 385: 329–332

41 Blackman D K, Cann J R, Janssen B, et al. Origin of extensional core complexes: Evidence from the Mid-Atlantic Ridge at Atlantis Fracture zone. J Geophys Res, 1998, 103: 21315–21333

42 Escartin J, Mevel C, Macleod C J, et al. Constraints on deformation conditions and the origin of oceanic detachments: The Mid-Atlantic Ridge core complex at 15°45′N. Geochem Geophys Geosyst, 2003, 4: 1–37

43 Escartin J, Smith D K, Cann J, et al. Central role of detachment faults in accretion of slow-spreading oceanic lithosphere. Nature, 2008, 455: 790–794

44 Cannat M, Cheadle M J, Mendel V, et al. Modes of seafloor generation at a melt-poor ultraslow-spreading ridge. Geology, 2006, 34: 605–608

45 Macleod C J, Searle R C, Murton B J, et al. Life cycle of oceanic core complexes. Earth Planet Sci Lett, 2009, 287: 333–344

46 Escartin J, Canales J P. Detachment in oceanic lithosphere: Deformation, magmatism, fluid flow, and ecosystems. Eos Trans AGU, 2011, 92: 31

47 Liu C J, Zhang L L, Yang L Y, et al. Formation of gabbronorites in the Purang ophiolite (SW, Tibet) through melting of hydrothermally altered mantle along a detachment fault. Lithos, 2014, 205: 127–141

Structure of the Baimarang massif in the Xigaze ophiolite, Yarlung Zangbo Suture Zone, southern Tibet, China

LI Yuan[1], LI RuiBao[2], DONG TianCi[3], YANG ShengBiao[3] & PEI Lei[3]

[1] *Centre of Continental Dynamics, Institute of Geology Chinese Academy of Geological Sciences, Beijing 100037, China;*
[2] *School of Earth Sciences and Resources, Chang'an University, Xi'an 710054, China;*
[3] *School of Earth Sciences and Resources, China University of Geosciences, Beijing 100083, China*

A predominance of mantle peridotites over mafic rocks in the Tibetan Xigaze ophiolite distinguishes it from other classic ophiolites in the Tethyan belt, such as the Semail massif of Oman. Despite the abundance of new petrological, geochemical, geochronological and isotopic data on ophiolites that have accumulated over the last few decades, there is still no consensus on the tectonic setting and dynamic mechanisms of formation of these enigmatic bodies. This study involved detailed, large-scale mapping of the well-preserved Baimarang massif in the western part of the Xigaze ophiolite in order to provide key constraints on its tectonic setting.

We demonstrate here that the Baimarang massif has a domal structure obviously different from most classic ophiolites. The massif is primarily cored by fresh harzburgites, locally containing small bodies of dunite, and dolerite intrusives. The fresh harzburgites have a well-developed foliation that dips northwest at angles of 60° to 80° and an associated spinel lineation. Mylonitic serpentinites invaded by dolerite intrusives occur on both the northern and southern sides of the fresh harzburgite. The transition between the fresh harzburgite and the mylonitic serpentinite is gradational and is marked by continuously increasing dolerite intrusives. The foliation in the northern mylonitic zone dips N to NW at angles of 50°–70°, whereas that in the southern belt dips SE at angles of 60°–70°. Most of the dolerite intrusives in the southern mylonitic belt are either irregular or lenticular in form. The shear sense in the dolerites indicates that the serpentinites were deformed by normal faulting, down to the south. In the upper part of the serpentinite belt a rare shear zone containing mylonitized harzburgite dips southwestward at angles of 50°–70°. The shear sense in this zone also indicates a southward movement. Partly surrounding the ultramafic core and serpentinite belt is a sequence of dolerite intrusives with an average thickness of 2 km, overlain by an extrusive sequence typically less than 500 m thick. The mafic rocks have undergone localized brittle deformation.

On the basis of our detailed study of the Baimarang massif, we conclude that it consists of three zones: a core of fresh harzburgite that underwent plastic deformation at high temperature, a middle unit of mylonitic serpentinite characterized by ductile deformation, and an upper cover of mafic intrusives and extrusives showing only brittle deformation. We suggest that the structure of the Baimarang massif is analogous to that of oceanic core complexes along slow-spreading mid-ocean ridges or in forearc basins.

Xigaze ophiolite, structures of ophiolite, oceanic core complex, extensional structures, detachment

doi: 10.1360/N972016-00203